Intramolecular rate process: Isomerization dynamics and the transition to chaos[a)]

Nelson De Leon and B. J. Berne

Department of Chemistry, Columbia University, New York, New York 10027
(Received 12 March 1981; accepted 18 June 1981)

The Hamiltonian flow of a system of two degrees of freedom, capable of undergoing geometrical isomerization, is studied as a function of the coupling between the reactive and unreactive degrees of freedom. The reaction dynamics are analyzed from the perspective of the KAM theorem and the transition to chaos. Conditions are found for the validity of linear rate laws and RRKM theory in isolated molecules.

I. INTRODUCTION

Geometrical isomerization can be described by the motion of a reaction coordinate (often an internal angle) in a double or multiple potential well. For isomerization to occur, an isolated molecule must suffer an activating collision with a photon or another particle.[1] In a very dilute gas or in a molecular beam, the time between successive collisions may be made very long on the time scale of molecular vibrations. The subsequent dynamics of the activated molecule under collisionless conditions is of considerable interest. If the reaction coordinate is not coupled to other intramolecular degrees of freedom, the motion over the barrier will be periodic, rate constants will not exist, and the usual linear rate laws will be invalid. When the reaction coordinate is coupled to other intramolecular degrees of freedom, energy exchange between modes may or may not give rise to a linear rate law. If the coupling is sufficiently weak, the dynamics will still be quasiperiodic and will be described by motion on many dimensional invariant tori in phase space.[2] In this KAM regime the usual rate laws will be invalid. It is shown here that for weakly coupled two-dimensional systems, for energies above the barrier, the tori can be subdivided into two distinct classes: *trapping tori* (TT) and *crossing tori* (CT). Motion on TT corresponds to librations in one or another well with no crossing of the barrier. Motion on CT corresponds to periodic crossing of the barrier with no trapping. As the "coupling"[3] is made stronger, there is a transition to "chaos" in which a measurable subset of CT are destroyed, but in which the TT are preserved. In this region, motion over the barrier cannot get trapped in any of the wells. An important consequence of this is that again rate constants will not exist and the linear rate law will be invalid. As the coupling is further increased, more and more of the CT are destroyed until all of them are finally destroyed; only then do TT start getting destroyed. At this point, some of the trajectories which pass over the barrier get trapped for periods of time in one or another of the wells. This is a necessary condition for the existence of rate constants, and for the validity of linear rate laws. We are still uncertain as to whether it is a sufficient condition because, even though the motion is irregular, it displays a great deal of coherence whenever the trajectory visits regions of phase space near undestroyed TT. For very strong coupling, almost all the CT and TT are finally destroyed. The trajectories are then highly stochastic. In this regime it is clear that rate constants exist, and moreover can be determined.

It follows from the foregoing that when the reaction coordinate is coupled strongly enough to other intramolecular degrees of freedom that a large measure of TT and all CT are destroyed, energy exchange between the modes can give rise to linear rate laws, and well-defined rate constants. If there is very rapid equipartitioning of the energy between these modes, it might be expected that the RRKM theory applies, and that the rate constant can be computed using purely statistical arguments. For illustrative purposes consider motion on the potential energy surface given in Fig. 1. The reaction can be described phenomenologically by

$$A \underset{k_b(E)}{\overset{k_f(E)}{\rightleftharpoons}} B ,$$

where $k_f(E)$ and $k_b(E)$ are the forward and backward rate constants at total energy E. Relaxation kinetics determines the kinetic rate constant

$$1/\tau_{Rxn} \equiv k_f(E) + k_b(E) . \tag{1}$$

This is the rate constant in the exponential time decay of an initial deviation from equilibrium. This rate constant in the RRKM theory is[4]

$$1/\tau_{\mathrm{RRKM}} = (X_A X_B)^{-1} \langle \dot{y}(0)\delta[y(0) - y_c]\theta[\dot{y}(0)]\rangle_E , \tag{2a}$$

where X_A and X_B are the equilibrium mole fractions of A and B, y_c is the value of the reactive coordinate (ordinate in Fig. 1) corresponding to the barrier maximum, $\dot{y}(0)\delta[y(0) - y_c]$ is the flux over the barrier, and $\theta(\dot{y})$ is the unit step function specifying that $\dot{y} > 0$. The step function counts only trajectories moving from A to B. The $\langle \cdots \rangle_E$ indicates an average over a microcanonical ensemble. According to Eq. (1), all trajectories initially passing over the barrier and moving from A to B contribute to the rate constant—even trajectories that might during the next instant, recross the barrier.

The RRKM rate constant depends on an equilibrium microcanonical average and thus does not depend on the molecular dynamics. The true rate constant depends on the dynamics and only under special circumstances will RRKM theory describe the chemical dynamics.

Because RRKM theory plays a very important role in the theory of chemical kinetics and in the interpretation

[a)]Work supported by a grant from the National Science Foundation (NSF CHE 79-07820).

 0021-9606/81/193495-16$01.00

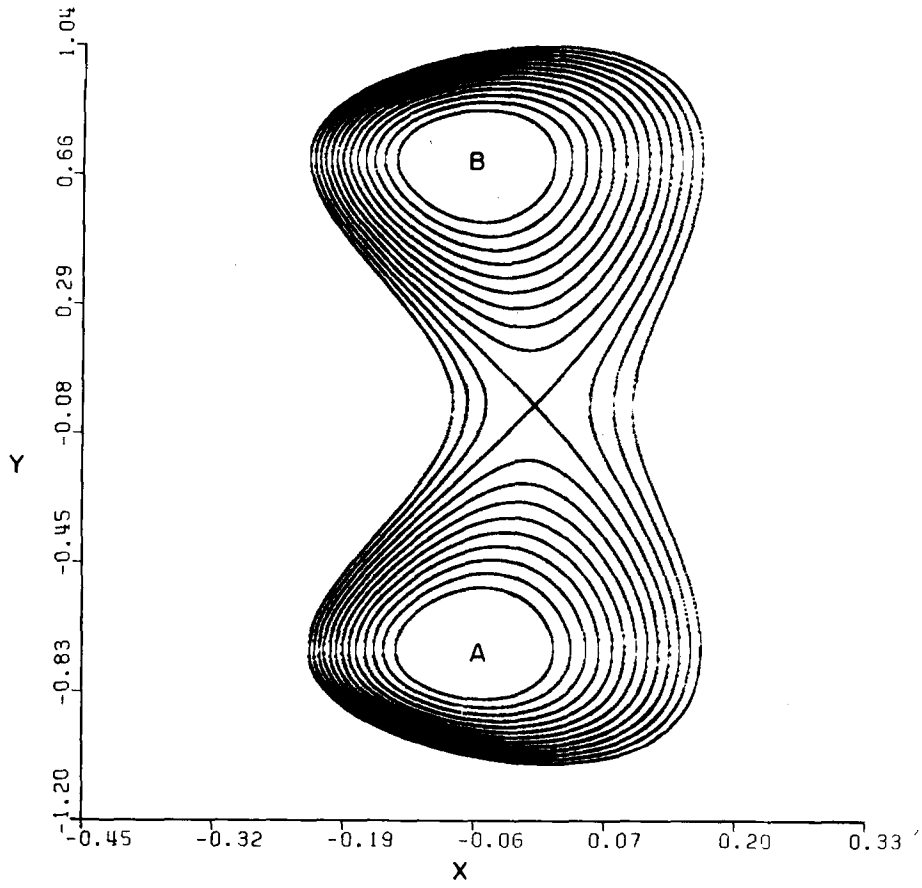

FIG. 1. A representative potential energy surface for the Hamiltonian [cf. Eq. (6)]. The parameters for this particular surface are $z = 2.30$ and $\lambda = 1.95$. The transition state is located at $Y = 0$. The reactants and products are labeled A and B.

of experiments, it is worth considering the circumstances under which it breaks down. If conditions are such that the energy hypersurface $H(\Gamma) = E$ is metrically decomposable into regular and irregular regions, then any given trajectory crossing the barrier will not be able to visit some measurable regions of phase space. The motion will then be nonergodic and any statistical theory, such as RRKM which assumes ergodicity will be in error. It is nevertheless possible to pose a modified statistical theory in which it is assumed that all states in the irregular part of phase space are "equally probable." The details are given in Appendix A. This leads to a rate constant $1/\tau_{BD}$ for a symmetric double well

$$\frac{1}{\tau_{BD}} = \frac{\Omega(E)}{\Omega_{\rm irr}(E)} \left(\frac{1}{\tau_{\rm RRKM}}\right) , \tag{2b}$$

where we assume that all crossing tori have been destroyed by the coupling, and where

$$\Omega(E) = \int_{\rm all\,\Gamma} d\Gamma \delta\,[E - H(\Gamma)] \tag{3a}$$

$$\Omega_{\rm irr}(E) = \int_{\rm irreg.\Gamma} d\Gamma\, \delta[E - H(\Gamma)] \tag{3b}$$

are, respectively, the full density of states at energy E and the density of states counting only the irregular region of the energy hypersurface. Obviously

$$\Omega_{\rm irr}(E) < \Omega(E) \tag{4}$$

and

$$1/\tau_{BD} > 1/\tau_{\rm RRKM} . \tag{5}$$

In this modified RRKM theory it is assumed that a trajectory starting at the barrier can visit all parts of the irregular region of phase space, i.e., the motion in the irregular region must be "ergodic" in the sense that the trajectory spends equal times in irregular regions of equal measure.

Even in a system where all the trajectories are irregular, RRKM theory becomes a poor approximation if there is correlated motion across[2(b)] the barrier, or if there are short-time recrossings of the barrier. (Even in fully stochastic models of barrier crossing there can be substantial deviations from RRKM theory.) Then the rate constant will depend on dynamics, and will not be given by a statistical theory or our modification of it.

It is the aim of this paper to clarify the conditions under which isomerization dynamics in isolated molecules gives rise to unimolecular rate laws and rate constants. Moreover, it is of interest to ascertain when, if ever, statistical theories such as the RRKM theory apply.

To apply the above questions, we study the dynamical behavior of a classical system with the Hamiltonian

$$H = 4(\dot{x}^2 + \dot{y}^2) + 4y^2(y^2 - 1)e^{-\varepsilon\lambda x} + \lambda_3\,(1 - e^{-\lambda x})^2 + 1 . \tag{6}$$

The potential[5] represents a quartic bistable potential (in y) with energy barrier $e^{-\varepsilon\lambda x}$ coupled to a Morse oscilla-

tor (in x). The coupling arises from the dependence of the barrier height[3] on x, the displacement from equilibrium of the Morse oscillator. Energy is measured in units of the barrier height corresponding to $x=0$. λ_3 is the dissociation energy of the Morse oscillator in these units and λ is the range parameter of the Morse potential. The quartic has two minima (stable points) at $y=\pm 1/\sqrt{2}$ and a maximum (metastable point) at $y=0$. These extremal points, and therefore the saddle point ($x=0$, $y=0$) do not depend on x. In what follows, we fix $\lambda_3 \equiv 10$. This is consistent with our expectation that in any real molecule, the dissociation energy will be much larger than the barrier to internal rotation. Thus we will study the Hamiltonian flow as a function of the coupling parameter z and the Morse parameter λ.

The potential energy surface for a representative choice of the parameters (z, λ) is shown in Fig. 1. Our aim is to study isomerization ($A \underset{k_b}{\overset{k_f}{\rightleftharpoons}} B$). Towards this end we define the isomeric state A and B such that if $y<0$, the system is in state A and if $0<y$, the system is in state B. As we shall see, for certain choices of the parameters, the system can get trapped in either well A or B for very long times compared with the period of vibration in these walls. Thus very long and accurate trajectories will be required to study the infrequent crossing of the barrier. How then can these rate processes be studied efficiently? Fortunately, there already exists a method of analysis based on the fluctuation dissipation theorem.[4,6,7] A simple extension of this to the microcanonical ensemble allows us to define the reactive flux at energy E as

$$k(t;E) \equiv \langle \dot{y}(0)\, \delta[y(0)]\, \theta[y(t)] \rangle_E \,. \tag{7}$$

Here the brackets $\langle \cdots \rangle_E$ indicate a microcanonical average at energy E; $\dot{y}(0)\,\delta[y(0)]$ is the initial flux over the barrier ($y_c=0$), and $\theta[y(t)]$, the step function, is unity at time t the system is in isomeric state B and zero if it is not.

As discussed elsewhere,[4,6,7] if at very long times (compared to the vibrational periods) $k(t;E)$ decays as a single exponential, then a unimolecular rate law will be valid, rate constants (k_f, k_b) will exist, and the decay rate of this exponential (τ_{Rxn}^{-1}) will be equal to $(k_f + k_b)$ as in Eq. (1). Furthermore, in general, the limit of the reactive flux $k(t \to 0+; E)$ can rigorously be shown to be the equivalent of the RRKM rate constant [cf. Eq. (2)].

To compute the reactive flux, one simply (microcanonically) samples initial phase points such that in all of them, the system is at $y(0)=0$. The trajectories corresponding to these initial states can then be used to determine the reactive flux. (See Appendix B for details.) In addition, since each of these trajectories originates at $y=0$, it is possible to determine the first time at which they recross $y=0$. The distribution of first passage time $p(\tau)$ can then be determined, and from this distribution, the fraction $W(\tau)$ of trajectories which have not made a first passage between 0 and τ can be determined. These distributions give further insight into the reaction dynamics. For example, from the unimolecular rate law, it is possible to show that a molecule will remain trapped in a well for time τ with probability $e^{-k\tau}$, where k^{-1} is the mean lifetime in the well. The rate law therefore implies that the trapping times are "randomly" distributed. Any deviation from a random distribution indicates a breakdown of RRKM theory and possibly unimolecular phenomenology.

In this paper we provide a full dynamical study of the simple two-dimensional system described by the Hamiltonian given by Eq. (6). It is remarkable that when the coupling between the reactive coordinate and the Morse oscillator is sufficiently large that the whole energy hypersurface is irregular, RRKM theory accurately describes the dynamics. However, when the coupling is such that a measurable set of trapped tori survive, the exact rate constants deviate considerably from the prediction of Eq. (2), thus indicating that there are still strong dynamical correlations even in the irregular trajectories.

II. DYNAMICAL STRUCTURE

The potential energy surface for a representation set of parameters [cf. Eq. (1)], is shown in Fig. 1. The closer the total energy E is to the barrier ϵ_0, the narrower will be the width of the transition zone, and the tighter will be the bottleneck. Thus the trajectories should be more readily trapped as $E \to \epsilon_0$. This is indeed the case in stochastic dynamics, but in Hamiltonian systems, if the transition to chaos takes place at a finite energy above ϵ_0, there will not be trapping, no matter how close E gets to ϵ_0. In this case one will then observe more effective trapping at higher energies.

The dynamical behavior of the system is first studied as a function of the two parameters λ and z [defined in Eq. (6)] for a fixed total energy $E=1.02\,\epsilon_0$, slightly above the barrier ϵ_0. Representative trajectories in configuration space are given in Fig. 2 for different choices of λ and z. Systems A1 to B3 all display trajectories that cross the transition zone. We call these *crossing trajectories* (or reactive trajectories). Trajectory A1 is periodic. It is interesting to note that none of the crossing trajectories of the set A1 to B2 are capable of visiting all of the available configurational space. The set C1 to C3 corresponds to trajectories for the same system. C1 and C2 are periodic and do not cross the transition zone. These are examples of purely *trapped trajectories*. C3 is a crossing trajectory that looks quite stochastic. Figure 2 shows that the system is capable of exhibiting very rich dynamical behavior ranging from periodic crossing trajectories (A1) and periodic trapped trajectories (C1 and C2) to stochastic (nonperiodic or unstable) crossing trajectories (B3). Some of the crossing trajectories (B2) look quite coherent.

Representative microcanonical reactive fluxes [$k(t;E)$] [cf. Eq. (7)] are given in Fig. 3 corresponding to some of the systems in Fig. 2. The sampling procedure used to determine these fluxes is given in Appendix B. It is clear from Fig. 3 that $k(t;E)$ is sensitive to the parameters λ and z. One should note the long time exponential behavior exhibited by the fluxes B2, C1, and C2. In these systems, a linear rate law is valid. We shall

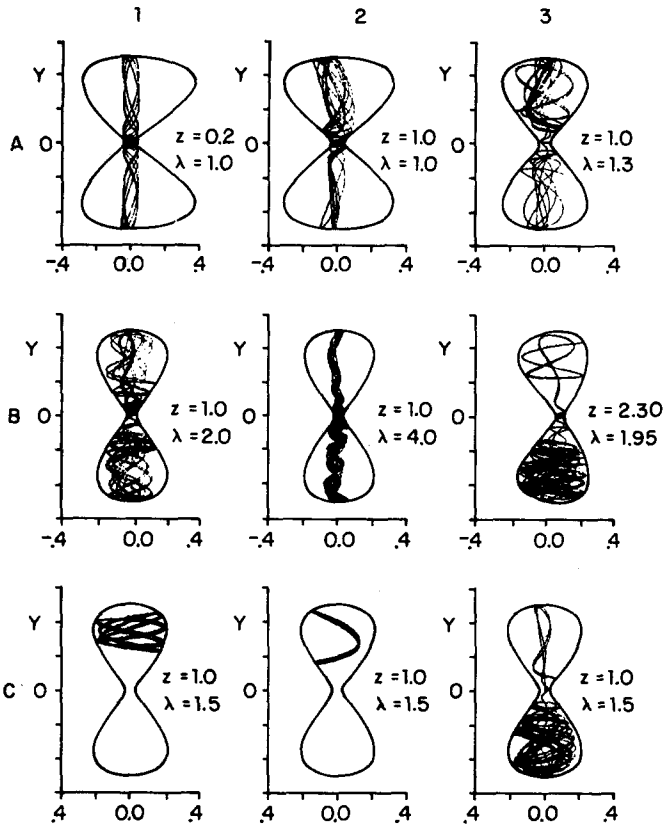

FIG. 2. In this figure, representative trajectories are mapped onto configuration space. A1 to B3 represent distinct systems. Note that the trajectory in system B3 is the only one in the set that tends to fill the entire available configuration space (given enough time). C1 to C3 show that in a given system there may be periodic trapped trajectories as well as irregular crossing trajectories. The abscissa and the ordinate correspond to the X and Y axis, respectively. One tic mark along the ordinate corresponds to 0.4 dimensionless units. In rows A and C, one tic mark along the abscissa corresponds to 0.2 dimensionless units. In B1, B2, and B3, one tic mark along the abscissa corresponds to 0.15, 0.08, and 0.14 dimensionless units, respectively.

discuss the detailed behavior of these fluxes later. Suffice it to say here that *phenomenological rate laws can be observed in reactive systems with as few as two degrees of freedom.*

The Hamiltonian of the system [Eq. (6)] can be expressed as

$$H = H_0(x) + H_0(y) + V(x,y)\,, \tag{8}$$

where

$$H_0(x) = 4\dot{x}^2 + \lambda_3[1-\exp(-\lambda x)]^2\,, \qquad \lambda_3 \equiv D_0/\epsilon_0\,, \tag{9a}$$

$$H_0(y) = 4\dot{y}^2 + 4y^2(y^2-1) + 1\,, \tag{9b}$$

$$V(x,y) = 4y^2(y^2-1)[\exp(-z\lambda x) - 1]\,. \tag{9c}$$

The classical motion of the unperturbed nonlinear oscillators $H_0(x)$ and $H_0(y)$ can be solved analytically. It is important to note that only $H_0(y)$ is independent of the parameters λ and z. Thus as λ and z are varied, most of the structural deformation of the potential surface will occur along the nonreactive degree of freedom x.

It is interesting to note that the ratio of the frequency of the uncoupled Morse oscillator to that of the uncoupled bistable oscillator is

$$R_\omega = \lambda_3^{1/2}\left(\frac{1-\sqrt{(E-1)/\lambda_3}}{2\omega_B^0}\right)\lambda \tag{10}$$

Taking $\lambda_3 = 10$, $E = 1.02$, and ω_B^0 just below the barrier, gives

$$R_\omega \cong 3.5\lambda\,. \tag{11}$$

This gives us a "ballpark" estimate of the number of oscillations of the Morse oscillator, corresponding to one oscillation of the reactive degree of freedom. As we shall see, the qualitative behavior of our system can be correlated with R_ω.

In discussing Hamiltonian flows in nonlinear dynamics it has proved useful to map the trajectories onto particular two-dimensional surfaces. These Poincare surfaces of section (PSS) reveal the underlying dynamical structure of the system. In this paper we define a surface of section not previously introduced in the literature. It is

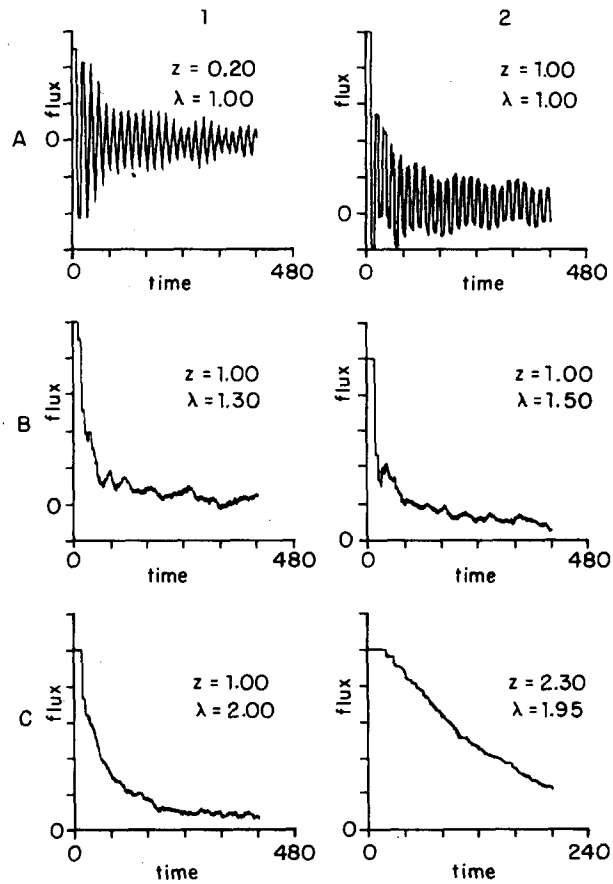

FIG. 3. Representative reactive fluxes: each flux corresponds to a distinct system as labeled. Typical trajectories contributing to each flux are shown in Fig. 2. The behavior of the various fluxes and their corresponding crossing (reactive) trajectories should be compared. In Fig. A1 one tic mark along the flux axis corresponds to 0.4 dimensionless units and 0.2 units in the rest.

simply a mapping of the trajectories onto a configuration plane rather than onto the usual coordinate–conjugate momentum plane. It is constructed as follows: when the Morse oscillator is at a turning point $\dot{x}=0$, the position of the system (x,y) is recorded by a point in configuration space. The advantage of this "configurational surface of section" (CSS) is that it readily gives a physical picture of what parts of configuration space a trajectory may visit.

Consider the CSS of Fig. 4 corresponding to the totally uncoupled system ($z=0$). The outer contour in this figure corresponds to the equipotential $V=E=1.02\epsilon_0$. The energies in the x and y degrees are separately conserved. Each trajectory has a mapping which is a pair of approximately parallel lines (dots if the trajectory is followed for finite times). The x component of these two lines gives the turning points of the Morse oscillator. Such a pair of lines corresponds to a two-dimensional invariant torus in phase space (defined by two isolating integrals of motion). Motion on these tori is periodic or quasiperiodic. We note that these tori can be subdivided into two classes: *crossing tori* (CT) and *trapped tori* (TT). On the former, $y(t)$ periodically moves back and forth across the barrier, whereas on the latter $y(t)$ is trapped forever in either well. The trapped tori each consist of a pair of parallel lines that are separated by a distance Δx greater than the x width of the saddle point region, as indicated on Fig. 4.

We are now ready to study what happens to the structure of these invariant manifolds in CSS as the coupling z is turned on. The questions one might ask are:

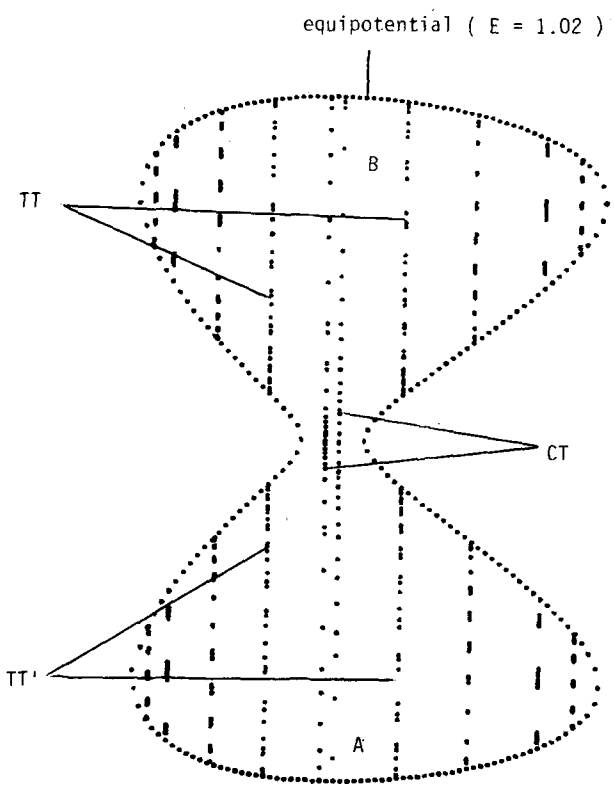

FIG. 4. Configuration surface of section (CSS): this example of a configurational surface of section corresponds to the uncoupled system ($Z=0$) at an energy $E=1.02\epsilon_0$ and $\lambda=1.0$. TT and TT′ correspond to trapped tori, and CT corresponds to a crossing torus.

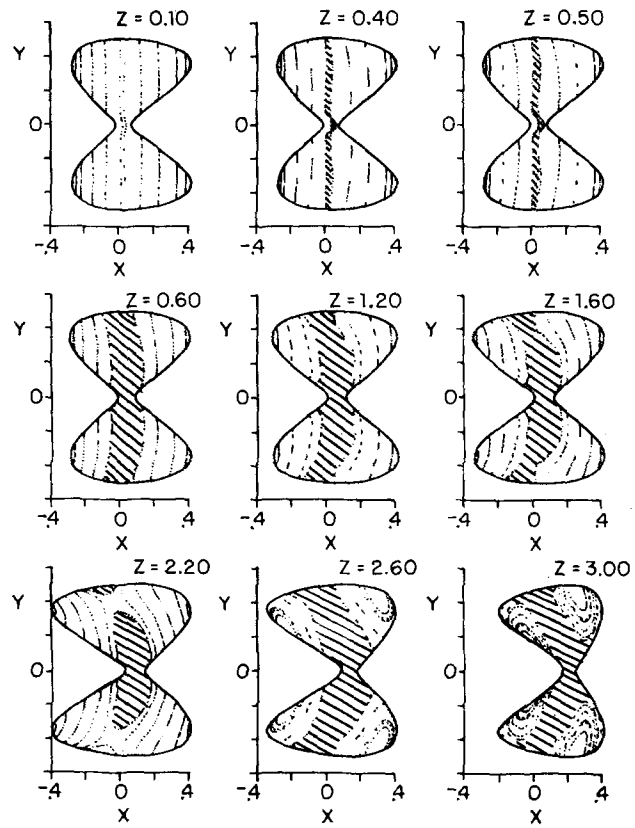

FIG. 5. A series of configurational surfaces of section are displayed. The various systems are at a total energy of $1.02\epsilon_0$ with the same Morse parameter λ (=1.0), and varying perturbation strength Z. Hatched regions correspond to regions of configuration space accessible to unstable reactive trajectories. The region outside the hatched zone is filled with trapped tori, and is thereby inaccessible to crossing trajectories. One tic mark along the Y axis corresponds to 0.4 dimensionless units.

(i) At a given energy ($E=1.02\epsilon_0$), how does the structure of CSS change (a) with perturbation strength z at fixed λ or (b) with λ at fixed perturbation strength z?

(ii) Which tori break up first, CT or TT, and why?

(iii) For fixed z and λ, how does the CSS change with total energy E?

(iv) What role is played by these manifolds in determining the dynamical structure of the reactive flux $k(t;E)$ and therefore in the reaction dynamics?

These questions are now addressed *seriatum*.

A series of CSS corresponding to $E=1.02\epsilon_0$, $\lambda=1$, and z varying between $z=0$ and $z=3$ (z cannot be increased beyond $z\cong 3.3$. Otherwise, the potential will become dissociative at energies close to the barrier) are shown in Fig. 5. At small z, all the tori persist, but are slightly deformed, as expected from the KAM theorem. The tori that first deform are those crossing tori (CT) that come close to the saddle point ($y=0$, $x=0$). These trajectories also come close to the mini-

ma ($y = \pm 1/\sqrt{2}$, $x = 0$). Crossing tori (CT) further away from the saddle point and all the trapping tori are relatively unaffected. Because the TT encompass only the well minima, they are much more stable to the perturbation. Thus for small z, only CT in a small strip going through the transition zone are perturbed. When the coupling is made large enough ($z \sim 0.40$), the "relatively unstable CT" are destroyed and the motion in this region of phase space ceases to be quasiperiodic and becomes irregular or stochastic. The regions corresponding to destroyed tori are indicated by a hatched strip in Fig. 5. As z is increased further, the hatched area gets wider until at about $z = 0.6$ it becomes wider than the transition zone. It is at this point that trapping tori start getting destroyed. Thus for $z > 0.6$, one finds a significant number of reactive trajectories that can get trapped. Recall that because of the delta function in $k(t;E)$ [cf. Eq. (7)], all trajectories contributing to the reactive flux must start at the transition state. It then follows that if the zone of stochasticity is wider than the transition zone, then all trajectories contributing to $k(t;E)$ are in the hatched region. In this case the motion contributing to $k(t;E)$ is no longer quasiperiodic. Further increase in z does not seem to widen the unstable zone, but it does significantly distort the equipotential and associated KAM surfaces (tori).

The above dynamical structure of CSS allows us to draw several conclusions:

(1) The phase space of an isolated, weakly coupled system exhibiting isomerization is decomposable into crossing tori (CT) and trapping tori (TT).

(2) CT are less stable (this may stem from the fact that CT encompasses a hyperbolic point resulting in a region of negative Riemannian curvature) than TT. Thus for intermediate coupling only a subset of the CT are destroyed. The TT are preserved, and the motion over the barrier, although irregular, never exhibits trapping.

(3) For strongly coupled systems, a measurable set of TT get destroyed, and crossing trajectories can get trapped. In this case, it is important to recognize that these irregular trajectories can visit only those regions of phase space not occupied by tori. This "excluded volume" effect may introduce strong correlations in the system.

(4) Increasing z at fixed λ has a limited effect on the system. In Fig. 4, varying z over its full range for $\lambda = 1$ does not destroy all the TT.

Let us now turn to question [i(b)]. How does the system behave with λ at fixed $E(=1.02\epsilon_0)$ and $z(=1.0)$? The coupling $z = 1$ is strong enough that in all of these sections there is a stochastic region (indicated by a cross-hatched region). A quick view of Fig. 6 shows that as λ is varied from 0.1 to 4.7 the region of stochasticity grows, shrinks, grows, and then shrinks again. From Eq. (11) it is seen that when λ is very small, y varies very rapidly compared to x; thus y can adiabatically follow x. When λ, and correspondingly R_ω, is very large, the converse is true, and x can adiabatically follow y. In both these extremes an adiabatic invariant will exist and the energy hypersurface

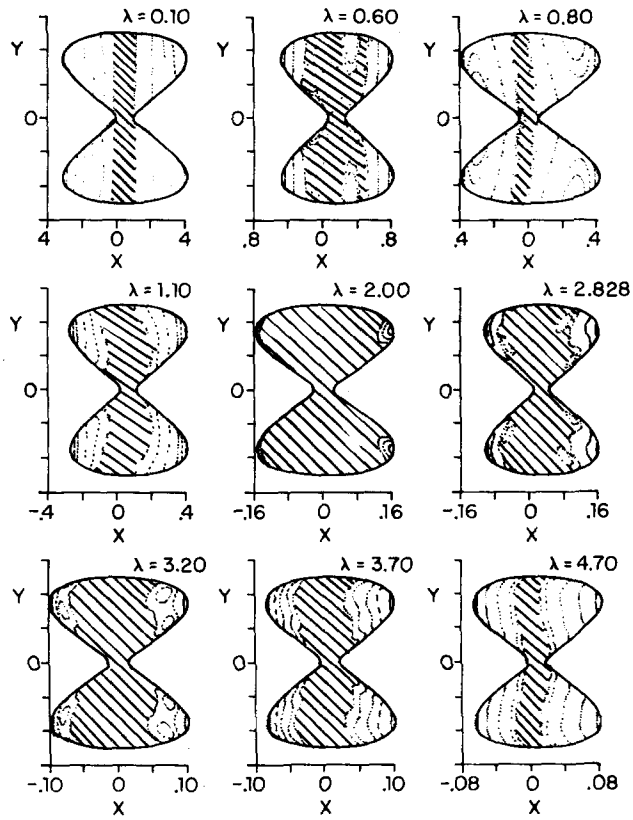

FIG. 6. A series of configurational surfaces of section are displayed. The various systems are at a total energy of $1.02\epsilon_0$, with the same value of the perturbation strength Z (= 1.0), but varying λ. The hatched regions are explained in Fig. 5. One tic mark along the Y axis corresponds to 0.4 dimensionless units.

should be filled with tori. This is precisely what is found, although it is not indicated in the figure. As one moves from the adiabatic region corresponding to low R_ω, the tori near the barrier are first deformed and a thin ribbon of stochasticity sets in. This region grows as R_ω is increased further, becoming a substantial fraction of the section around $\lambda = 2.00$. We expect that as R_ω is further increased, the region of stochasticity will decrease until finally for very high R_ω when adiabadicity sets in, the plane is filled with tori. Actually, there is a region around $0.6 < \lambda < 1.0$ when the stochasticity diminishes and then increases. This behavior is rather unexpected and merits further study.

The results of Fig. 6 can be summarized by the following:

(5) Frequency variations (λ variations) have a much more pronounced effect on the dynamical structure than do increases in the perturbation strength z.

(6) If in the uncoupled system one mode is much faster than the other mode, then in the coupled system the two modes will be adiabatically decoupled.

(7) We can expect to see linear rate laws in systems in which there is a high degree of stochasticity; that is, in systems where the natural periods in the decoupled system do not differ too much.

Let us now address question (iii), by studying the CSS

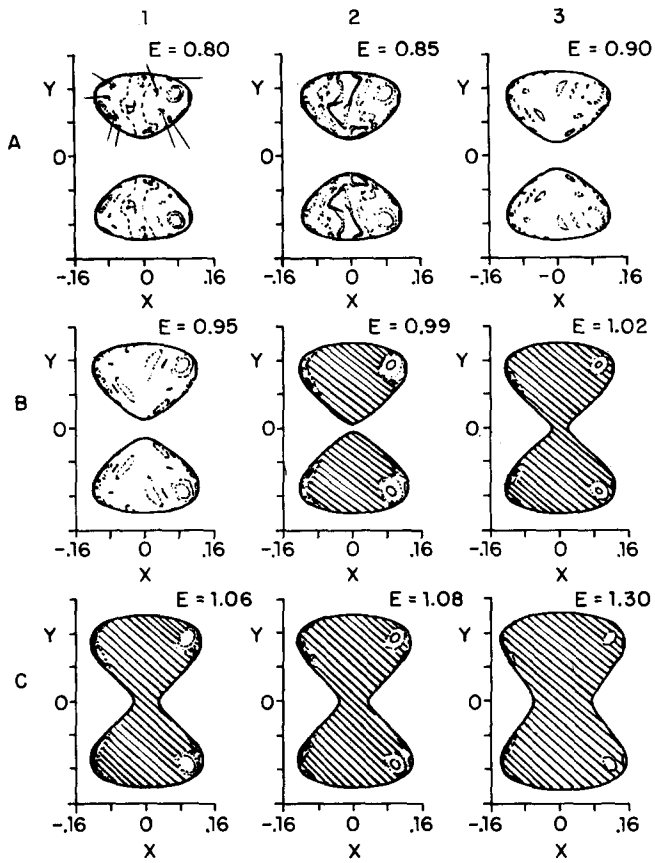

FIG. 7. A sequence of configurational surfaces of section are shown for a system with varying total energy E, but for fixed $\lambda = 2.5$ and $Z = 1.0$. A very complicated structure is apparent at energies below the barrier. The critical energy for this system is about $0.83\epsilon_0$. The arrows in Fig. A1 point to a series of islands signifying that unstable motion should soon be expected. One tic mark along the Y axis corresponds to 0.4 dimensionless units.

for fixed $z(=1.0)$ and $\lambda = (2.5)$ as a function of total energy. The critical energy for this system is found to be approximately $E_c = 0.83\epsilon_0$ in this paper, we have only examined limited range of (λ, z, E) space. The results presented are qualitatively representative. The critical energy was found by investigating the usual $(y, \dot{y})$ Poincare surface of section. In Fig. 7 we present CSS for E slightly below E_c, up to $E = 1.30\epsilon_0$. For $E = 0.80\epsilon_0$, well below the barrier, the system is integrable, tori exist, but the structure is quite complicated, consisting of island chains (indicated by arrows in Fig. 7(A1). Thus we expect that unstable motion will occur for energies nearby. Increasing E above $0.83\epsilon_0$ leads to small unstable regions (not shown here). A large fraction of CSS becomes irregular only at energies slightly below $E = \epsilon_0$. Further increase in E does little to alter the extent of chaotic motion. What is more important is to notice how the width of the transition zone changes with energy. It is simple to show that the width of the transition zone is given by

$$[\Delta x(E, \lambda)]_{TS} = -\lambda^{-1} \ln\left[\frac{1 - \sqrt{(E-1)/\lambda_3}}{1 + \sqrt{(E-1)/\lambda_3}}\right] . \quad (12)$$

From this we find that the width at $E = 1.30\epsilon_0$ the width is nearly four times the width at $E = 1.02\epsilon_0$. The ratio of $[\Delta x]_{TS}$ to the width of the well $(y = \pm 1/\sqrt{2})$, is denoted by

$$\psi(E, \lambda) = [\Delta x(E, \lambda)]_{TS} / [\Delta x(E, \lambda)]_{well} . \quad (13)$$

This can be computed analytically (for $z = 0$, 1, and 2). It is a very strong function of E. In Fig. 8 we see the effects of ψ on the reactive flux. Clearly, ψ will become smaller the closer E is to ϵ_0, and the tighter will be the bottleneck. The converse is true. In a purely stochastic theory, one would expect trapping times to be longer as ψ becomes smaller (and for very small ψ one would expect RRKM rate constants). Note how, with increasing E, the reactive flux becomes oscillatory.

It is now reasonable to ask if we can correlate the extent of stochasticity of the system at $E = 1.02\epsilon_0$ with the critical energy (energy at which measurable stochastic-

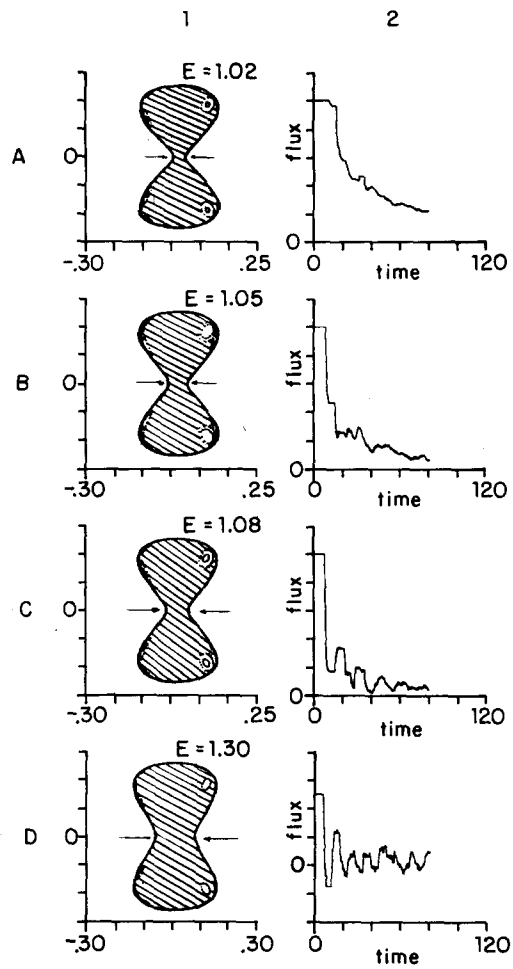

FIG. 8. A sequence of configurational surfaces of section and the corresponding reactive fluxes are shown as a function of total energy E. The series corresponds to the system discussed in Fig. 7. Arrows indicate the width of the transition zone. The reactive flux changes dramatically as the transition state zone widens [cf. Eq. (13)] with increasing energy. Note that the measure of irregularity is approximately constant throughout the energy range of interest. In column 1, one tic mark along the Y axis corresponds to 0.4 dimensionless units. One tic mark along the flux axis is 0.2 units in A2, B2, and C2, and 0.4 units in D2.

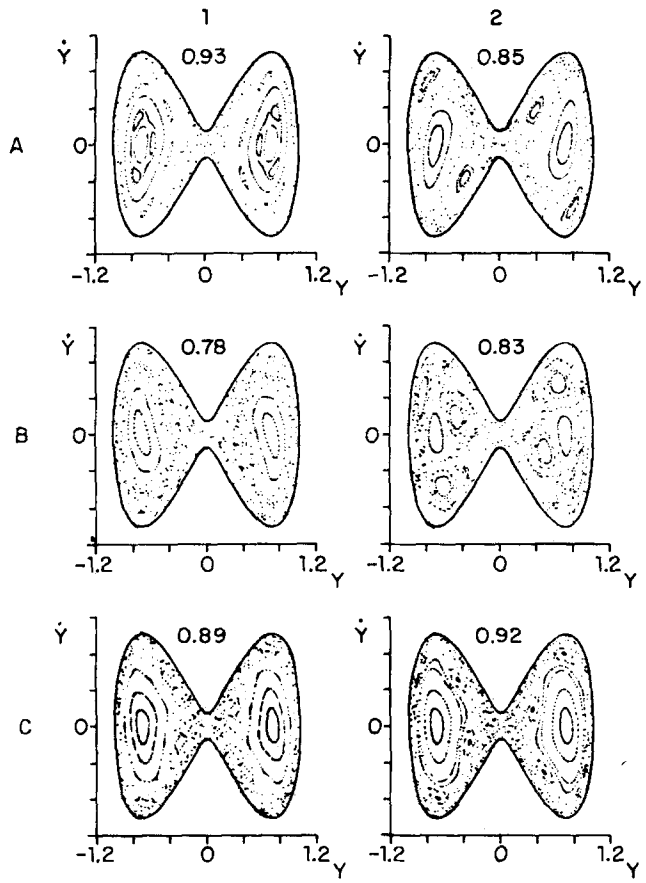

FIG. 9. The Poincare surface of section: Y versus $\dot{Y}$ for $X = 0$ and $\dot{X} > 0$. These sections are all at a total energy of $1.02\epsilon_0$. The various systems all have $Z = 1.0$, but different values of λ. In A1, $\lambda = 1.3$; in A2, $\lambda = 1.5$; in B1, $\lambda = 2.0$; in B2, $\lambda = 2.5$; in C1, $\lambda = 2.828432$; in C2, $\lambda = 3.0$. The critical energy for each system is given in each figure. The lower the critical energy, the more chaos one can expect just above the barrier. For the most highly stochastic system we found (system B3 of Fig. 2), the critical energy was less than $0.1\epsilon_0$. The corresponding surface of section at $1.02\epsilon_0$ appears to be a shotgun pattern. One tic mark along the ordinate corresponds to 0.2 dimensionless units.

ity is first observed) of the system. To this end, in Fig. 9, we present the usual (y versus $\dot{y}$) Poincare surface of section for several systems. This figure suggest a "rule of thumb" observation: the lower the critical energy, the larger the extent of stochasticity one can expect to find just above the barrier. In view of previous literature, this result is not unexpected, but it is important to correlate it with isomerization dynamics. This leads us to the following conclusion:

(8) Roughly, the lower E_c for the system, the larger the measure of "stochasticity" just above the barrier. This leads to a correlation between the motion well below the barrier with that just above it. The theoretical prediction of E_c can be of substantial value in determining whether or not a system will be highly stochastic above the barrier and, concommitantly, whether or not linear rate laws are valid.

In this section we have shown that the degree of stochasticity, and the critical energy E_c are sensitive functions of the parameters. Clearly when a measurable set of trapped tori exist, the amplitude of the Morse oscillator on any crossing trajectory is constrained to be within a well-defined strip, and the energy that can be transferred to this oscillator has an upper bound considerably smaller than the total energy E. Clearly, the magnitude of the energy that can be transferred from the reactive to the unreactive mode is limited. Intuitively, we expect that the rate constant for isomerization is inversely proportional to the mean time that the crossing trajectories remain trapped. If after crossing the barrier, the trajectory can only lose a small amount of energy to the nonreactive degree of freedom (the x oscillator), then it should be able to regain this energy (through a fluctuation) rather quickly, and the trapping time will be short. The smaller the measure of trapped tori, the larger the amount of energy transfer, and the longer it should take to regain the energy. *Thus the rate constant should decrease as the measure of trapped tori decreases.* This intuitive argument contains many hidden assumptions. In point of fact, it is quite similar to our modification of the RRKM theory embodied in Eq. (2), where the integrals are over the irregular region of phase space—the region in which the energy transfer is limited. (In the canonical transition state theory, the rate constant which is usually proportional to $e^{-\beta\epsilon_0}$ would be proportional to $e^{-\beta(\epsilon_0-\epsilon_m)}$, where ϵ_m is the lower bound on the energy that can be found in reactive degree of freedom.) This theory also leads to a prediction that the rate constant should decrease as the measure of trapped tori decreases. These arguments incorporate the metric decomposability of phase space, i. e., the breakdown of ergodicity, into a statistical theory of rate constants. What we have learned in this section is how the coupling affects the structure of phase space and the measure of tori, and we are thus better able to compute generalized RRKM rate constants. Implicit in all the statistical theories of the rate constant is an assumption that motion within the irregular part of phase space is ergodic. In fact, there are varying degrees of stochasticity, ranging from nonergodic, ergodic, weak mixing, mixing, K system, C system, etc.[8] Thus the trajectories may have a high degree of correlation so that a simple statistical ansatz may be totally unjustified. Thus, it will come as not great surprise that the above prediction that the rate constant should decrease as the measure of trapped tori decreases is totally at odds with the results of this study. We address the reaction dynamics in the next section.

III. REACTION DYNAMICS

It has been shown that the simple Hamiltonian system [Eq. (8)] has a very rich dynamical structure. It is of considerable interest to relate the isomerization dynamics in this system to the structure in phase space as indicated in the CSS. The reaction dynamics in a representative set of systems are summarized in Fig. 10. Column 1 gives a set of CSS at $E = 1.02\epsilon_0$, corresponding to different parameter choices (λ, z). Column 2 gives a set of representative crossing trajectories. Column 3 gives a set of microcanonical reactive fluxes and column 4 gives a set of first passage time distributions as dis-

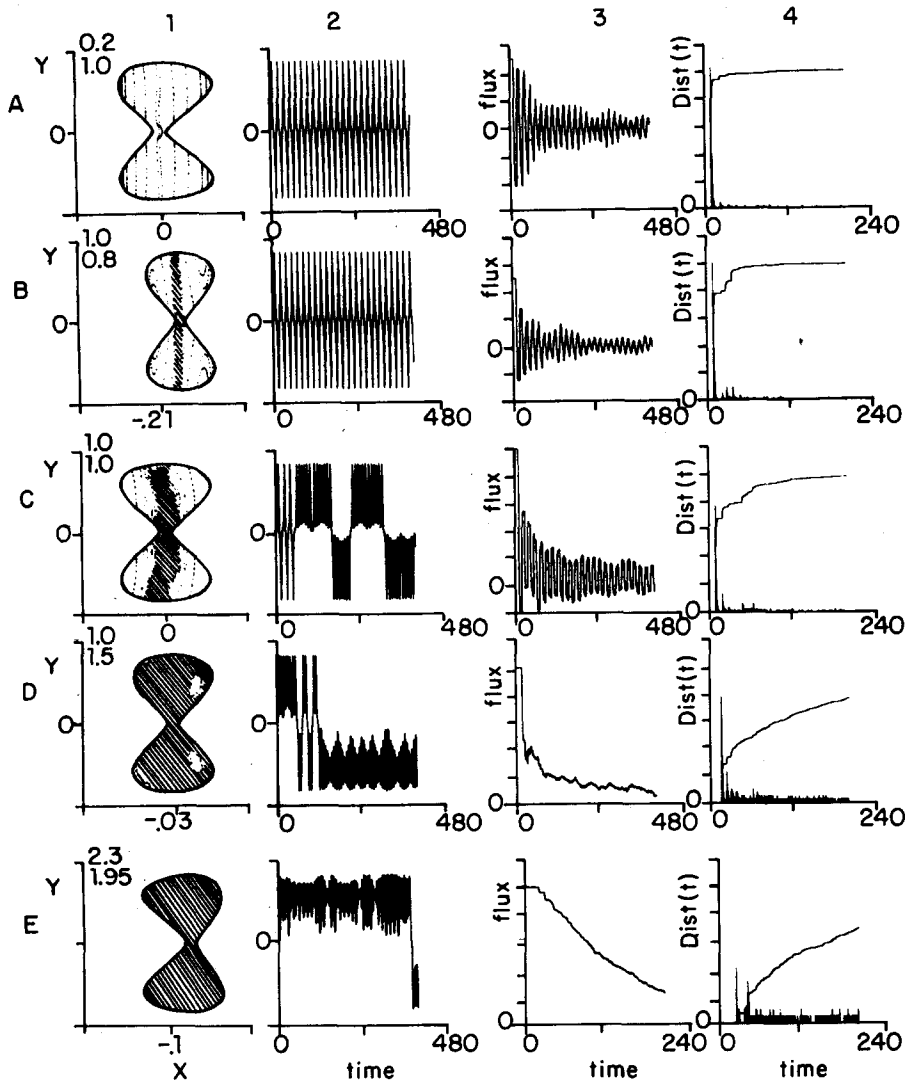

FIG. 10. Overview of representative system; a comparison of the configurational surface of section, the time evolution of the reactive coordinate $Y(t)$, the flux, and the distribution of first passage times $W(t)$ are given. Along the ordinate, one tic mark corresponds to 1.2 units in columns 1 and 2, 0.4 units in A3 and B3, and 0.2 units in C3, D3, and $E3$. In column 4 the units along the ordinate are arbitrary. The upper left-hand corner of column 1 gives the values of z (top) and λ for each system.

cussed earlier. Each row corresponds to a given system (λ, z) in the CSS. As one goes from row A to row E, the systems become more stochastic, i.e., the coupling strength increases. System A is weakly coupled; all the trajectories are regular, and the phase space (or CSS in A1) is entirely decomposable into crossing tori (CT) and trapping tori (TT). The representative trajectories are quasiperiodic, and a typical crossing trajectory has the reactive coordinate periodically crossing the barrier as shown in Fig. 10(A2). In system B, the coupling is strong enough to destroy "all" of the crossing tori; thus the crossing trajectories must be irregular; nevertheless, the reaction coordinate looks rather periodic [Fig. 10(B2)]. In neither system A nor B do we observe trapping. In system C the coupling is strong enough to destroy some TT. This should be obvious from the fact that the stochastic strip is now wider than the transition zone. Now the representative trajectory moves across the barrier and gets trapped for many librational periods before recrossing the barrier. The librational motion looks coherent. In system D, a very large measure of the TT are destroyed, the representative trajectory gets trapped for long periods of time, but there still seems to be a great deal of coherence in the trapped motion. Finally in system E, all the tori are destroyed. Now the crossing trajectory gets trapped for a very long period of time and, moreover, the librational motion looks very chaotic.

It is clear from column 2 that in systems C and D the crossing trajectories are irregular; but, nevertheless, portions of the trapped motion look quite coherent. These trajectories show a very high degree of correlation, e.g., when the system crosses the barrier, it seems to recross it several times, but when it gets trapped, it seems to librate quite coherently. Could this arise because these trajectories evolve on some remnants—so to speak—of a crossing torus and then switch over to a remannt of a trapping torus? It is almost as if the irregular trajectory is captured for a time by the surviving tori and moves under their influence, i.e., moves, so to speak, on a "vague torus."[9] Should this be the case, then as more and more trapped tori are destroyed, the coherence and concomittant long correlation times should disappear. In Fig. 10 (E2), we see that the reactive trajectory looks very random—very much like it would if it was strongly coupled to a heat bath. Here no tori

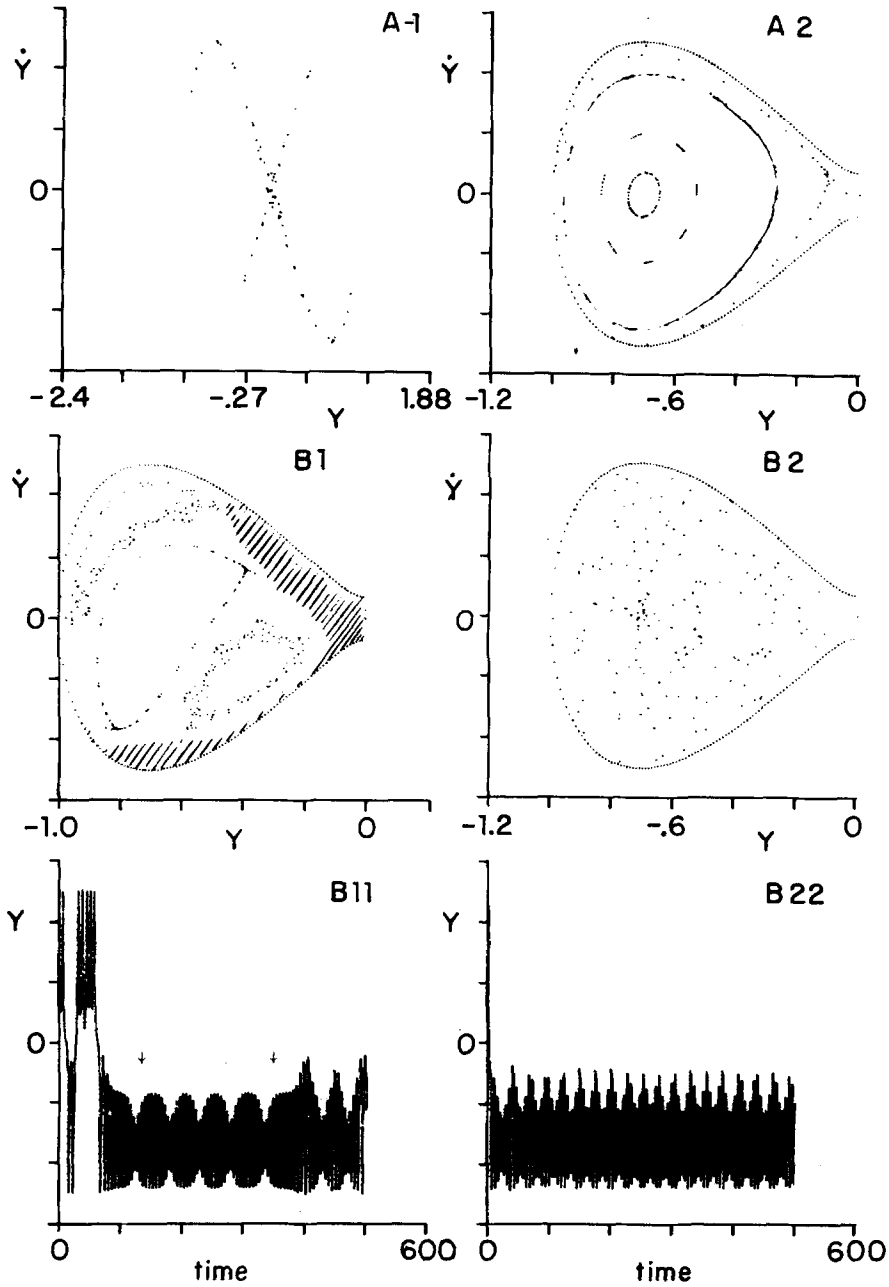

FIG. 11. The surface of section in A2, B1, and B2 correspond to only the reactant "A" side of the potential energy surface. In B1, A and B correspond to distinct trapped tori [A is the inner torus (oval) and B corresponds to the outer two ovals]. These A and B tori correspond respectively to trajectories of the type C1 and C2 in Fig. 2. The trajectories B11 and B22 were used to obtain the "vague" tori A and B B1, respectively. The arrows in B11 indicate where the trajectory was "cut" in order to obtain the section. Note the regularity of the amplitudinal motion in both cases—even though they are "supposed" to be irregular. One tic mark along the ordinate in Figs. B11 and B22 correspond to 0.4 units. All other tic marks along the ordinate are 0.2 dimensionless units.

survive, so the irregular crossing tori never fall under the influence of tori and the motion is very chaotic.

To test these ideas, we show in Fig. 11 the usual Poincare surface of section (PSS). Here the trajectories are mapped onto the $(y, \dot{y})$ plane whenever $x=0$, $\dot{x}>0$. In Fig. 11(A1) we show the mapping of the irregular crossing trajectory [cf. Fig. 10(B)] onto the PSS. The irregular behavior ocurrs mainly near the saddle point. The motion is nevertheless quite coherent, and the mapping looks, in fact, very similar to a pure crossing torus in the uncoupled system. In Fig. 11(A2) the solid curve indicates the outer trapped torus. The dots are the mapping onto the PSS of the irregular crossing (reactive) trajectory given in Fig. 10(C). It should be noted that during this period of time, the irregular trajectory follows the trapped torus very closely. The motion is quite coherent. In Fig. 11(B1), the regions [described as Eqs. (A) and (B) in the figure caption] define two topologically distinct tori. The dots about region A and B are formed by the two independent trajectories 11(B11) and 11(B22), respectively. Only the very regular part of trajectory 11(B11) (the part between the arrows) was used to obtain the dots on the PSS. The fact that these two irregular trajectories seem to move for very long periods of time, in a very localized region of phase space, is surprising. This short time structure so closely resembles motion on a surviving torus that this can be called a vague torus. Though not shown here, other trajectories seem to "jump" periodically from the A torus to the B torus. Trajectories influenced by tori in A or B execute many periods before wandering away and visiting the hatched regions in Fig. 11(B1). In the

visiting the hatched regions in Fig. 11(B1). In the hatched region, the motion becomes more chaotic. The amplitude $y(t)$ then becomes more irregular. Could it be that the hatched areas contain regions of negative Riemanian curvature?[10] This decomposition is approximate in that eventually a trajectory starting in one such region does indeed visit the other region. Nevertheless, the long correlation times associated with this motion arises from the "inhomogeneity" of the irregular part of the energy hypersurface. Lastly, in Fig. 11(B2) the mapping of the very "stochastic" trajectory of Fig. 10(E) is shown. This is the typical "shotgun" pattern usually associated with the stochastic instability.[11] Here no evidence of dynamical structure is observed. These observations appear to suggest the existence of vague tori and lead us to the following conjecture:

(9) Systems in which not all the invariant tori are destroyed have a measurable set of irregular trajectories, that spend finite, and relatively long, periods of time executing almost regular motion. This quasiregular motion occurs when the trajectories visit irregular regions of phase space neighboring existing tori. Approximate invariants may exist in these regions—hence they have been called vague tori. Trajectories in these regions are quite stable and lead to long correlation times and trapping times.

The reactive flux $k(t;E)$ [cf. Eq. (7)], corresponding to Fig. 10 were each computed by averaging over microcanonically sampled trajectories. These are presented in Figs. 10(A3)–10(E3). The trajectories were computed using the De integrator based on the Adams–Moulton algorithm.[16] Integration accuracy was monitored by conservation of total energy with percent error $=0.01$, and by time reversal. The computations were carried out in double precision on a VAX 11/780 computer. The sampling techniques and other details of the calculation will be discussed in Appendix B.

Since each of the trajectories originates at $y=0$, it is possible to determine the first time at which they recross $y=0$, and thereby the distribution of first passage times $p(\tau)$, and the corresponding fraction $W(t)$ $\equiv 1-\int_0^t dt\, p(\tau)$, of trajectories which do not make their first passage before time t. These are given in Figs. 10(A4)–10(E4).

This histograms $[p(\tau)]$ show that there is a minimum time for first passage. This corresponds to the shortest time for traversal of a well at the fixed energy E. Moreover, they show that there are fairly well-defined narrow short time peaks. These represent the trajectories that do not get trapped but instead recross the transition state quickly, and with a very small dispersion in first crossing times. This is expected in systems with weak coupling, where the system is not stochastic, but it should be noted that there is a remnant of this rapid recrossing even in the systems in which all reactive trajectories are stochastic. The fraction of trajectories that rapidly recross decreases as the coupling increases; nevertheless, even in very stochastic systems, there is a high degree of coherence typified by the narrow peak. In addition, we see that the distribution of "long first passage times" is quite broad. The probability of not making a first passage in time t is also given in Figs. 10(A4)–10(E4). In the fully stochastic system, the long time behavior of this distribution looks quite exponential—a result consistent with a "random" or Poisson distribution of first passage times—a signature of a unimolecular rate law. In the less stochastic systems, the long time behavior is consistent with a sum of two or more exponentials, so that only at times much longer than given in Figs. 10(B4)–10(D4) will it be possible to determine the rate constant. The reason for this long time behavior appears to be that the trajectories seem to get coherently trapped for very long times on "vague trapping tori." Thus an accurate determination of the long time decay might give smaller values of $1/\tau_{Rxn}$ than are reported here.

TABLE I. Comparison of the decay rate $1/\tau_{rxn}$ to the RRKM prediction $1/\tau_{RRKM}$, and the short time inverse first passage time $1/\tau_{fp}$. If the short time $1/\tau_{fp}$ is to reveal the phenomenological rate constant, then $1/\tau_{rxn}=2/\tau_{fp}$. Agreement is attained only in the last two systems. Both are highly stochastic. The RRKM prediction is only correct for the last system. System 8, though highly stochastic, was found to have a vestige of trapped tori—which would indicate the reason for its deviation from the RRKM prediction.

z	λ	τ_{rxn}^{-1}	τ_{fp}^{-1}	τ_{RRKM}^{-1}
1.000	1.300	•••	•••	0.0073
1.000	1.500	0.004±0.001	0.0050	0.0073
1.000	2.000	0.004±0.0005	0.0057	0.0073
1.000	2.500	0.005±0.001	•••	0.0073
1.000	2.828	0.005±0.0015	•••	0.0073
1.000	3.350	0.006±0.002	•••	0.0073
1.125	2.310	0.0059±0.0005	•••	0.0073
2.500	2.020	0.0057±0.0005	0.0028	0.0070
2.300	1.950	0.0075±0.0005	0.0040	0.0070

The reactive flux given in Figs. 10(A3)–10(E3) are completely consistent with the above discussion. When there is weak coupling, $k(t;E)$ exhibits a decay due to dephasing. Each reactive trajectory is essentially periodic in $y(t)$, but there is a distribution of periods [given by the sharp peaks of $p(\tau)$]. As the coupling gets stronger, the first peak in $p(\tau)$ decreases and the fraction of trajectories giving rise to random recrossing times grows. Since the former gives heterogeneous oscillatory decay, and the latter "exponential" decay, the flux behaves something like the superposition of these two kinds of decays. The behavior is of course more complicated than this description would imply. Thus in the case of strong couplings the long time decay is exponential and a rate constant can be extracted. In Table I we give the values of the kinetic rate constant τ_{Rxn}^{-1}, determined from the reactive flux, along with the corresponding RRKM values τ_{RRKM}^{-1}, and values of the inverse mean first passage times τ_{FP}^{-1} calculated from the long-time behavior of $p(\tau)$. Because the trajectories used to determine $k(t;E)$ were much longer than those used to determine $p(\tau)$, the values of τ_{Rxn}^{-1} determined from the reactive flux were judged to be more accurate than those determined by fitting $W(t)$ to $\exp(-t/2\tau_{Rxn})$. Only for the most stochastic systems do we get agreement between these methods, i.e., $\tau_{Rxn}^{-1}=2\tau_{FP}^{-1}$.

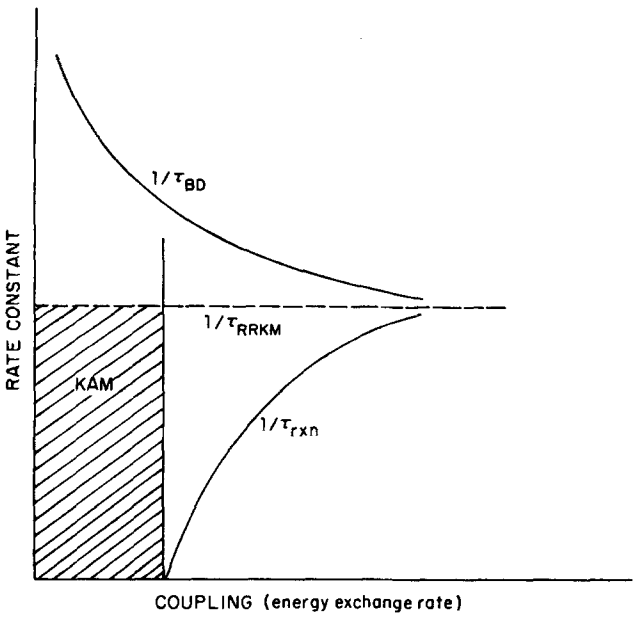

FIG. 12. A schematic diagram of the dependence of the reaction rate $1/\tau_{rxn}$ on the coupling strength (or energy exchange rate). The curve labeled $1/\tau_{rxn}$ refers to the long time exponential decay rate determined from the reactive flux. $1/\tau_{RRKM}$ refers to the rate predicted from RRKM theory. It is not sensitive to coupling strength (see Table I). The term "coupling strength" should not be confused with perturbation strength.[3] $1/\tau_{BD}$ is the rate predicted by the statistical theory (RRKM-like theory) applied only to the irregular part of the energy hypersurface. See Eq. (A7b) and Appendix B.

The τ^{-1}_{RRKM} were computed analytically from Eq. (2). It should be noted that *there is agreement between* τ^{-1}_{Rxn} *and* τ^{-1}_{RRKM} *only for the most stochastic systems*. Clearly, when the measure of trapped tori is nonzero, the reactive trajectories are restricted to a subregion of the energy hypersurface and the density of states used in RRKM overcounts the reactive states. Then RRKM will be a very poor approximation. As discussed in Sec. I and Appendix A, the statistical theory can be modified by considering the irregular region of phase space; cf. Eq. (2) and Eq. (A7). The modified rate constants τ^{-1}_{BD} satisfies the inequality given by Eq. (5). Thus we expect that as the coupling (stochastic region) increases, $(\tau_{BD})^{-1}$ decreases until it eventually becomes equal to τ^{-1}_{RRKM}. This happens when the whole energy hypersurface is stochastic. It is $(\tau_{BD})^{-1}$ which gives an upper bound on the actual rate constant τ^{-1}_{Rxn}. From Table I we see that τ^{-1}_{Rxn} increases with stochasticity. Thus neither the full nor the modified RRKM (TST) theory accounts for the "experimental" results when there is not full stochasticity. The situation is summarized schematically in Fig. 12. Instead, the rate constant τ^{-1}_{Rxn} depends on dynamical properties (like the energy exchange rate). This bears a close resemblance to what happens in stochastic theories where the rate constant depends on dynamic properties like the collision rate or friction coefficient, and only becomes equal to the transition state value under rather restrictive conditions. Another possible explanation is that in the less stochastic systems, motion on vague tori give rise to long trapping times.

The above observation can be summarized as follows:

(10) The measure (in the Lebesgue sense) of the irregular part of the energy hypersurface must be close to the measure $\mu(E)$ of the constant energy surface, i.e., a significant fraction of the TT must be destroyed, before one can expect to observe linear rate laws.

(11) For very strongly coupled systems, i.e., systems in which all the tori are destroyed, a unimolecular rate law pertains, rate constants exist, and these rate constants are moreover very well approximated by RRKM (transition state) theory.

(12) In less strongly coupled systems, i.e., systems in which trapping tori still exist, it appears that a unimolecular rate law describes the behavior of the reactive trajectories, but now the rate constants are not approximated by the full RRKM theory. A modified RRKM theory taking account of the restricted density of states corresponding to the stochastic region of phase space, gives very poor agreement with the dynamics. In fact, we find that $1/\tau_{Rxn}$ increases with stochasticity, whereas $1/\tau_{BD}$ decreases with stochasticity.

(13) At intermediate coupling there appears to be a high degree of correlation in the irregular trajectories. This correlation seems to be related to the regions of phase space still occupied by tori. When an irregular trajectory comes near a region occupied by tori, it behaves coherently; when it is in regions free of tori, it behaves chaotically. Motion on vague tori can lead to very long trapping times, and highly correlated motion.

In the foregoing, it has been shown how the behavior of the reactive flux can be correlated with the dynamical structure in phase space. All of the systems studied have the same total energy $E = 1.02\epsilon_0$.

In Fig. 7, it was shown how the CSS for a given system ($z = 1$, and $\lambda = 2.5$) varied with total energy E. It should be noted that systems 7(B3), 7(C1), 7(C2), and 7(C3) are almost entirely stochastic. In Fig. 8, we show how the reactive flux decays for each of these systems. As one goes down the column from system 8(A) to 8(D), the width of the transition zone increases dramatically. The corresponding reactive fluxes show a significant change in behavior, clearly due to the effect of increased ψ [cf. Eq. (13)]. For system A the flux decays exponentially at long times. For systems B and C the flux acquires much more dynamical structure and oscillatory behavior, and for system D no discernable long time decay exists; there is no separation in time scales and a linear rate law does not apply, even through the extent of stochasticity is more or less constant. Clearly then, even for a fully stochastic system when the energy is "too high," a rate constant will not exist. A detailed analysis of this energy dependence shows that as the total energy is increased, the trapping time decreases, because the width of the transition zone increases and the bottleneck effect becomes less pronounced.

Since the canonical reactive flux is

$$k(t;T) = \frac{\int dE\Omega(E)k(t,E)e^{-\beta E}}{\int dE\Omega(E)\,e^{-\beta E}} \quad , \tag{14}$$

it follows that the dominant contribution to the rate constant stems from energies close to the barrier height. This means that one will see a linear rate law, exponentially decaying flux only at low temperatures.

IV. DISCUSSION

Even in systems consisting of only two degrees of freedom, it has been shown here that nonlinear coupling can give rise to a unimolecular rate law for isomerization and correspondingly to well-defined rate constants. It has also been shown that calculation of the long time decay of the reactive flux allows one to determine the rate constants—should they exist. This has been clearly shown for the most stochastic system (E) of Fig. 10 and in this case the RRKM rate constant (τ^{-1}_{RRKM}) is in excellent agreement with the rate constant determined from the reactive flux. The less stochastic systems B–D of Fig. 10, however, exhibit features which cannot be accounted for by a simple statistical theory. When the coupling is strong enough to destory some trapping tori, reactive trajectories do indeed get trapped for long periods of time. These trajectories are irregular but nevertheless display a great deal of coherence, i.e., there are very long correlation times. The trapping times appear to be nonrandom, and it would take a very long integration time to establish whether these systems are described by a unimolecular rate law with well-defined rate constants. It is possible that the very long time decay in these systems is not exponential—although we suspect it is. There are comparable cases in transport theory—such as Brownian motion in two dimensions—where phenomenological decay is not observed.[12] Nevertheless, we fit the long-time behavior of $k(t;E)$ to an exponential and report the decay constant in Table I. The reason for the long correlation times and long trapping times in these moderately coupled systems is rather difficult to pin down. What is clear is that a substantial fraction of the crossing trajectories in these systems, although irregular, spend considerable periods of time executing coherent or "regular" motion. These trajectories seem to fall under the influence of the trapping tori that still exist in the system. One consequence of this is that τ_{Rxn} seems to be a decreasing function of the coupling. This behavior is counterintuitive in that we expect the trapping time to increase as the stochasticity (measure of the irregular region of phase space) increases (cf. the discussion in Sec. I and Fig. 12).

That τ^{-1}_{Rxn} increases as the coupling increases is consistent with the following argument. In any coupled system energy is exchanged between the x and y oscillators. Let τ_E denote the correlation time of the energy fluctuation—should a correlation time exist. τ^{-1}_E plays a role in this problem somewhat similar to the collision rate, or friction constant in stochastic dynamic models of barrier crossing. In the event that $\tau_E \gg T$, where T is the period of oscillation of a periodic crossing orbit, then a trajectory starting at the transition state will coherently or periodically recross the transition state for a time on the order of τ_E before losing enough energy to get trapped. It will remain trapped until it gains enough energy to recross the barrier. The time of trapping is thus also τ_E and $\tau_{Rxn} \propto \tau_E$ or $\tau^{-1}_{Rxn} \sim \tau^{-1}_E$. Thus we expect the kinetic rate constant τ^{-1}_{Rxn} to be an increasing function of τ^{-1}_E. Intuitively we expect τ_E to decrease and τ^{-1}_{Rxn} to increase as the coupling (stochasticity) increases, an expectation entirely in agreement with the observation. Of course, no evidence is given for the existence of τ_E. These considerations raise more questions than can be answered here, and further study is required.

It is interesting to note that recently Berry *et al.*[13] have conducted experiments to measure the rate constant for the molecule methyl isocyanide. The isomerization for this molecule is thought to pass through an intermediate indicated below:

$$CH_3CN \rightleftharpoons CH_3NC \ ,$$

$$CH_3{-}C{\equiv}N \rightleftharpoons \begin{array}{c} CH_3 \\ / \quad \backslash \\ C \equiv N \end{array} \rightleftharpoons C{\equiv}N{-}CH_3 \ .$$

It is of particular interest to us that their results indicated that at a total energy just above the barrier, the microcanonical rate constant agreed well with RRKM theory, but at a higher energy the RRKM prediction be came very poor. One might attempt to explain this behavior by the widening of the bottleneck effect discussed in Secs. II and III, in connection with Figs. 7 and Eq. (B). As we have at higher energies, the reactive flux becomes oscillatory and the rate constant does not exist.

The simple two-dimensional system presented here has a rather rich dynamical structure. The focus of this paper has been to clarify the relationship between a reaction dynamics and the dynamical structure associated with the KAM theorem. In fact we know no other work that discusses this relationship between the topology of phase space and rate constants for barrier crossing in bounded systems. Many of the conclusions outlined here form the basis for further investigations, e.g.,

(a) What happens when there are more than two degrees of freedom?

(b) What are the dynamics in a corresponding quantum system?

With regard to (a), it is important to elucidate the role of Arnold diffusion.[14] With regard to (b), it has already been shown that there is a transition to chaos in wave packet dynamics.[15] Nevertheless, this remains a controversial area. It also enables one to pose an exact quantum counterpart to the RRKM theory.

To summarize the major conclusions of this paper:

(1) When the coupling between the reaction coordinates and the oscillatory coordinate is large enough to destroy all the crossing tori and some trapping tori, crossing trajectories can get trapped.

(2) The closer the total energy is to the activation energy, the longer is the time spent by a trajectory librating in a well. Thus only for energies close to the activation energy will there be a separation in time scales between vibrational periods and trapping times. This

is a necessary but not sufficient condition for the existence of linear rate laws.

(3) For very strongly coupled systems, i.e., systems in which all the tori are destroyed [and condition (2) is obeyed], a unimolecular rate law pertains, rate constants exist, and the rate constants are very well approximated by RRKM (transition state) theory.

(4) Even in strongly coupled systems, when the energy is significantly larger than the activation energy, the reactive flux exhibits an oscillatory decay reminiscent of heterogeneous relaxation, and the system cannot be described by a linear rate law. At energies close to the activation energy, $1/\tau_{Rxn}$ behaves like $1/\tau_{\mathrm{RRKM}}$, i.e., it increases with energy, but at higher energy, it should deviate from RRKM theory and, moreover, should decrease with energy.

(5) In less strongly coupled systems, i.e., systems in which trapping tori still exist [when condition (2) above is satisfied], it appears that a unimolecular rate law describes the behavior of the reactive trajectories, but now the rate constants are not approximated by the full RRKM theory. A modified RRKM theory taking account of the restricted density of states corresponding to the stochastic region of phase space gives very poor agreement with the dynamics. In fact, we find that $1/\tau_{Rxn}$ increases with stochasticity, whereas $1/\tau_{BD}$ decreases with stochasticity.

(6) At intermediate coupling there appears to be a high degree of correlation in the irregular trajectories. This correlation seems to be related to the regions of phase space still occupied by tori. When an irregular trajectory comes near a region occupied by tori, it behaves coherently; when it is in regions free of tori, it behaves chaotically. Motion on vague tori can lead to very long trapping times.

It is interesting to note that comment (3) suggests that we explore the conditions under which all trapping tori are destroyed. Should we be able to find the dynamical conditions, we will be able to predict when RRKM should be valid.

APPENDIX A: GENERALIZATION OF RRKM THEORY TO NONERGODIC SYSTEMS

Phase space is decomposable into regular and irregular parts. Let us define a quantity $I(\Gamma)$ which has the property that

$$I(\Gamma)=\begin{cases}1, & \Gamma\in S_I,\\ 0, & \Gamma\notin S_I,\end{cases} \tag{A1}$$

where S_I is the measurable set of irregular points in phase space. Let us define the normalized microcanonical density in the subspace S_I as

$$\rho_I(\Gamma,E)=\frac{1}{\Omega_I(\Gamma)}\,\delta[E-H(\Gamma)]I(\Gamma), \tag{A2}$$

where

$$\Omega_I(E)=\int d\Gamma\, I(\Gamma)\delta[E-H(\Gamma)] \tag{A3}$$

is the density of irregular states at energy E. Let us now define the normalized auto correlation function of the fluctuation in product molecules

$$C_I(t;E)=\langle \delta N_B(0)\delta N_B(t)\rangle_{E,I}/\langle \delta N_B^2 I\rangle_{E,I}, \tag{A4}$$

where subscript E, I indicates an average over ρ_I, i.e., over the irregular part of phase space. The corresponding reactive flux is

$$k_I(t;E)=-\frac{dC_I(t;E)}{dt}=\frac{\langle \dot y(0)\delta[y(0)-y_c]\,\theta[y(t)]\rangle_{E,I}}{\langle \theta(y)\rangle_{E,I}[1-\langle \theta(y)\rangle]_{E,I}}. \tag{A5}$$

This follows from the uniformity of the propagator, and the stationarity of $\rho_I(\Gamma,E)$. The latter follows from the fact that I is a constant of the motion (a regular trajectory remains regular, and an irregular trajectory remains irregular, and never the twain shall meet). It is also easy to show that from symmetry $\langle \theta(y)\rangle_{E,I}=x_B=[1-\langle \theta(y)\rangle_{I,E})=x_A$. Every trajectory contributing to $k_I(t;E)$ is a crossing trajectory. The initial value of this reactive flux is

$$\frac{1}{\tau_{BD}}\equiv\lim_{t\to 0^+}k(t;E)=\frac{1}{x_A x_B}\langle \dot y\,\theta(\dot y)\delta(y-y_c)\rangle_{E,I}, \tag{A6a}$$

$$\frac{1}{\tau_{BD}}=\frac{1}{x_A x_B}\,\frac{\int d\Gamma I(\Gamma)\delta[E-H(\Gamma)]\dot y\,\theta(\dot y)\delta(y-y_c)}{\int d\Gamma\, I(\Gamma)\delta[E-H(\Gamma)]}. \tag{A6b}$$

If all the crossing trajectories are irregular then the I can be deleted from the numerator and

$$\frac{1}{\tau_{BD}}=\frac{1}{x_A x_B}\,\frac{1}{\Omega_I(E)}\int d\Gamma\,\delta(E-H)(\Gamma)\dot y\,\theta(\dot y)\delta(y-y_c), \tag{A7a}$$

$$\frac{1}{\tau_{BD}}=\frac{\Omega(E)}{\Omega_I(E)}\,\frac{1}{\tau_{\mathrm{RRKM}}}. \tag{A7b}$$

A statistical theory of the rate constant is formulated as follows: each trajectory originating at the transition state y_c gets trapped for a time (long compared to vibrational periods) in the well towards which it is initially moving. Then there are no rapid recrossings. A trapped trajectory can only recross after it regains energy from the other degrees of freedom (to which the energy was originally lost). The distribution of trapping times is assumed to be random. Then $C_I(t;E)$ must decay as a single exponential and since its initial decay rate is given by Eq. (A6), it follows that

$$k_I(t;E)=(1/\tau_{BD})\exp(-t/\tau_{BD}). \tag{A8}$$

Thus the decay rate of $k_I(t;E)$ is $1/\tau_{BD}$. If the whole energy hypersurface is irregular, then

$$\frac{1}{\tau_{BD}}\to\frac{1}{\tau_{\mathrm{RRKM}}}=\frac{1}{x_A x_B}\,\frac{1}{\Omega(E)}\int d\Gamma\,\delta(E-H)\dot y\,\delta(y-y_c)\theta(\dot y). \tag{A9}$$

Now in an experiment, suppose the initial states are microcanonically distributed according to $\rho(\Gamma)=\delta(E-H)/\Omega(E)$. Since

$$\rho(\Gamma)=\frac{[I+(1-I)]\delta(E-H)}{\Omega(E)}=\frac{\Omega_I(E)}{\Omega(E)}\rho_I(\Gamma,E)+\frac{\Omega_R(E)}{\Omega(E)}\rho(E), \tag{A10}$$

where $\Omega_R(E)=\Omega(E)-\Omega_I(E)$ is the density of regular

states and $\rho_R(\Gamma, E) = (1 - I)\delta(E - H)/\Omega_R(E)$.

The full fluctuation correlation function is

$$C(t, E) = \langle \delta N_B(0)\delta N_B(t)\rangle_E / \langle \delta N_B^2 \rangle_E \,, \tag{A11}$$

where the average is over the full energy hypersurface. Upon substitution of Eq. (A10), this can be expressed as

$$C(t) = [\Omega_I(E)/\Omega(E)]\, C_I(t;E) + [\Omega_R(E)/\Omega(E)]\, C_R(t;E)\} \,, \tag{A12}$$

where

$$C_R(t;E) = \frac{1}{x_A x_B} \int d\Gamma\, \delta[E - H(\Gamma)] \times [1 - I(\Gamma)]\, \delta N_B(0)\delta M_B(t)/\Omega_R(E) \,. \tag{A13}$$

↑ regular trajectories

Now if all crossing trajectories are irregular, none of the trajectories contributing to $C_R(t;E)$ can cross the barrier so that $C_R(t;E)$ is constant in time, i.e., $C_R(t;E) = C_R(0, E)$. It follows from Eq. (A12) that the reactive flux will then be

$$k(t;E) = -\frac{dC(t)}{dt} = \frac{\Omega_I(E)}{\Omega(E)}\, k_I(t;E) \,. \tag{A14}$$

Substitution of Eq. (A8) into Eq. (A14) then gives the reactive in the statistical theory

$$k(t;E) = \frac{\Omega_I(E)}{\Omega(E)}\, \frac{1}{\tau_{BD}}\, e^{-t/\tau_{BD}} = \frac{1}{\tau_{\mathrm{RRKM}}}\, e^{-t/\tau} BD \,, \tag{A15}$$

where the last equality follows from Eq. (A7b).

This shows that the exponential decay observed in a nonergodic system in which all crossing trajectories are irregular, is given by decay constant $1/\tau_{BD}$ defined in Eq. (A7b), and Eq. (2b). When there are TT,

$$1/\tau_{BD} > 1/\tau_{\mathrm{RRKM}} \,, \tag{A16}$$

but when the measure of all TT is zero,

$$1/\tau_{BD} = 1/\tau_{\mathrm{RRKM}} \,. \tag{A17}$$

It is important to note that the prefactor of the exponential in Eq. (A15) is $1/\tau_{\mathrm{RRKM}}$. Thus in general the statistical decay rate cannot be found from the initial time derivative of the full time correlation function.

APPENDIX B: PROCEDURE USED FOR EVALUATING REACTIVE FLUX

It is important to outline how the reactive flux is computed. The identity $\theta[\dot{y}(0)] + \theta[-\dot{y}(0)] = 1$ is substituted into Eq. (7) and the resulting terms are rearranged to give

$$x_A x_B k(t, E) = \langle \dot{y}\,\theta(\dot{y})\delta(y)\rangle_E F^{(+)}(t, E) + \langle \dot{y}\,\theta(-\dot{y})\delta(y)\rangle_E F^{(-)}(t, E) \,, \tag{B1a}$$

where

$$F^{(\pm)}(t;E) \equiv \int d\Gamma\, p^{(\pm)}(\Gamma;E)\theta[y(t)] \,, \tag{B1b}$$

and

$$p^{(\pm)}(\Gamma;E) \equiv \frac{\dot{y}\delta(y)\theta(\pm\dot{y})\delta(E - H)}{\int d\Gamma \dot{y}\,\delta(y)\theta(\pm\dot{y})\delta(E - H)} \,. \tag{B1c}$$

Because $p^{(\pm)}(\Gamma;E)$ are normalized probability distributions, it follows from the observations $\lim_{t\to 0^+} \theta[y(t)] = \theta(\dot{y})$ that

$$\lim_{t\to 0^+} F^{(+)}(t;E) = 1 \,, \tag{B2a}$$

$$\lim_{t\to 0^+} F^{(-)}(t;E) = 0 \,. \tag{B2b}$$

The coefficients of $F^{(\pm)}(t;E)$ in Eq. (B1a) are equilibrium microcanonical averages. Because H is quadratic in $\dot{y}$, transformation of variables from $\dot{y} \to -\dot{y}$ yields

$$\frac{1}{x_A x_B} \langle y\,\theta(-\dot{y})\delta(y)\rangle_E = \frac{1}{x_A x_B} \langle \dot{y}\,\theta(\dot{y})\delta(y)\rangle_E = +\frac{1}{\tau_{\mathrm{RRKM}}} \,. \tag{B3}$$

The last equality follows from Eq. (7). Upon substitution into Eq. (15a)

$$k(t;E) = \frac{1}{\tau_{\mathrm{RRKM}}} [F^{(+)}(t;E) - F^{(-)}(t;E)] \,. \tag{B4}$$

The quantities $F^{(\pm)}(t, E)$ are computed as follows. The initial values of x, $\dot{x}$, and $\dot{y}$ are sampled (for $y = 0$) from $p^{(\pm)}(\Gamma)$; and trajectories corresponding to each choice of initial conditions are generated. The normalized reactive flux

$$\hat{k}(t;E) \equiv \frac{k(t;E)}{k(t - 0^+;E)} = [F^{(+)}(t) - F^{(-)}(t)] \tag{B5}$$

is evaluated by averaging $\theta[y(t)]$ over these trajectories. This gives $\bar{\theta}_+[y(t)] - \bar{\theta}_-[y(t)]$. To evaluate the contributions from the stochastic region, we merely insert $I(\Gamma)\delta(E - H)$ in place of $\delta(E - H)$ in Eq. (B1c).

[1] W. Forst, *Theory of Unimolecular Reactions* (Academic, New York, 1973).

[2] (a) The role of the KAM theorem and the effects of chaos in dynamical systems has been discussed in connection with energy transfer dissociation in coupled oscillator systems. See the excellent reviews by D. W. Noid, M. L. Koszykowski, and R. A. Marcus, Phys. Chem. **32**, (1981); P. Brumer, Adv. Chem. Phys. (in press); M. Tabor, *ibid.* (in press); I. C. Percival, *ibid.* 36, 1 (1977); S. A. Rice, *ibid.* (in press). For an excellent introduction to the various concepts in nonlinear mechanics see J. Ford, Adv. Chem. Phys. 24, 155 (1972). (b) S. Nordholm and S. A. Rice, J. Chem. Phys. 62, 157 (1974).

[3] Used here, the term coupling is a rather complicated quantity. It depends on the two parameters z and λ. Space does not allow us to make a clear statement of this quantity. Suffice it to say that the term coupling as used here is proportional to the measure of the irregular region of phase space.

[4] D. Chandler, J. Chem. Phys. 68, 2959 (1978).

[5] This model springs from the expectation that the barrier to internal rotation in a real molecule will decrease when the bond connecting the rotation groups is stretched. For example, in ethane the barrier to rotation of CH_3 should decrease as the C–C bond is stretched. In butane, the barrier

in the *gauche* $\rightleftarrows$ *trans* isomerization should decrease as the C2–C3 bond is stretched or if the C–C–C angles are stretched.
[6]J. A. Montgomery, Jr., D. Chandler, and B. J. Berne, J. Chem. Phys. 70, 4056 (1979).
[7]R. O. Rosenberg, B. J. Berne, and D. Chandler, Chem. Phys. Lett. 75, 162 (1980).
[8]V. I. Arnold and Z. Avez, *Ergodic Problems of Classical Mechanics* (Benjamin, New York, 1968).
[9]W. Reinhardt (private communication).
[10]Yoji Aizawa, J. Phys. Soc. Jpn. 33, 1963 (1972); R. Kosloff and S. A. Rice, J. Chem. Phys. 74, 1947 (1981).
[11]M. Henon and C. Heils, Astron. J. 69, 73 (1964).
[12]J. H. Dymond and B. J. Alder, J. Chem. Phys. 52, 923 (1970).
[13]K. V. Reddy and M. J. Berry, Chem. Phys. Lett. 52, 111 (1977).
[14]M. A. Lieberman, *Nonlinear Dynamics* (New York Academy of Sciences, New York, 1980).
[15]M. J. Davis, E. B. Stechel, and E. J. Heller, Chem. Phys. Lett. 76, 21 (1980).
[16]L. F. Shampine and M. A. Gordon, *Computer Solution of Ordinary Differential Equations* (Freeman, San Francisco, 1975).